Proof-of-Principle Direct Measurement of Particle Statistical Phase

Yan Wang,[1,2,3] Matteo Piccolini,[4,5,*] Ze-Yan Hao,[1,2,3] Zheng-Hao Liu,[1,2,3] Kai Sun,[1,2,3,†]
Jin-Shi Xu,[1,2,3,‡] Chuan-Feng Li,[1,2,3,§] Guang-Can Guo,[1,2,3] Roberto Morandotti,[5]
Giuseppe Compagno,[6] and Rosario Lo Franco[4,¶]

[1]*CAS Key Laboratory of Quantum Information, University of Science and Technology of China, Hefei 230026,
China*
[2]*CAS Center for Excellence in Quantum Information and Quantum Physics, University of Science and Technology
of China, Hefei 230026, China*
[3]*Hefei National Laboratory, University of Science and Technology of China, Hefei 230088, China*
[4]*Dipartimento di Ingegneria, Università di Palermo, Viale delle Scienze, Palermo 90128, Italy*
[5]*INRS-EMT, 1650 Boulevard Lionel-Boulet, Varennes, Québec J3X 1S2, Canada*
[6]*Dipartimento di Fisica e Chimica - Emilio Segrè, Università di Palermo, via Archirafi 36, Palermo 90123, Italy*

The symmetrization postulate in quantum mechanics is formally reflected in the appearance of an exchange phase governing the symmetry of identical-particle global states under particle swapping. Many indirect measurements of this fundamental phase have been reported thus far, but a direct observation has been achieved only recently for photons. Here, we propose a general scheme capable of directly measuring the exchange phase of any type of particle (bosons, fermions, or anyons), exploiting the operational framework of spatially localized operations and classical communication. We experimentally implement it on an all-optical platform, providing a proof of principle for different simulated exchange phases. As a by-product, we supply a direct measurement of the real bosonic exchange phase of photons. Additionally, we analyze the performance of the proposed scheme when mixtures of particles of different nature are injected. Our results confirm the symmetrization tenet and provide a tool to explore it in various scenarios. Finally, we show that the proposed setup is suited to generating indistinguishability-driven NOON states useful for quantum-enhanced phase estimation.

I. INTRODUCTION

The symmetrization postulate divides particles living in a three-dimensional space into two groups: bosons and fermions. This postulate forces the state of an ensemble of identical bosons (fermions) to be symmetric (antisymmetric) under the exchange of any pair of particles [1]. If we consider a system of two identical particles, its global state must then satisfy $|\psi(1,2)\rangle = e^{i\phi}|\psi(2,1)\rangle$, where 1 and 2 refer to the two constituents and the relative phase ϕ is the particle exchange phase (EP), with $\phi = 0$ for bosons and $\phi = \pi$ for fermions. Furthermore, the existence of particles called anyons, living in two-dimensional spaces with a fractional EP $\phi \in (0, 2\pi) \setminus (\pi)$, has been suggested [2,3],

and has attracted the attention of the scientific community in recent decades [4–6]. This fundamental phase has been indirectly measured in various experiments [7–12]. Despite the fundamental importance of the symmetrization postulate in both understanding the quantum world and practical applications, only the bosonic nature of photons has so far been directly proven by use of a state transport protocol [13,14]. Direct observation of fermionic and anyonic EPs is still missing, leaving the field open to the introduction of techniques capable of filling this gap.

In the standard approach to identical particles [1], the global state vector is symmetrized or antisymmetrized with respect to unphysical labels associated with each constituent. This approach is known to exhibit drawbacks when one is trying to assess real quantum correlations between constituents [15,16]. Given the key role played by entanglement in quantum technologies, several different methods have been developed to fix this issue [16–23]. Among these, the no-label approach [21] has some advantages: it straightforwardly identifies physical entanglement and establishes its quantitative relation with the degree

———————
*matteo.piccolini@unipa.it
†ksun678@ustc.edu.cn
‡jsxu@ustc.edu.cn
§cfli@ustc.edu.cn
¶rosario.lofranco@unipa.it

of spatial indistinguishability [24]; the latter is associated with the spatial overlap of particle wave functions. Importantly, in the no-label formalism, the role played by the particles' nature does not manifest itself in the (anti)symmetrization of the quantum state, but instead in the probability amplitudes of the global system [21,22].

The no-label approach has been widely exploited in environments with spatially localized operations and classical communication (sLOCC) [23–31]. This procedure can be seen as a natural extension of the standard local operations and classical communication for distinguishable particles to the case of indistinguishable and individually unaddressable constituents. Operationally, sLOCC makes the global state of indistinguishable particles undergo a projective measurement over spatially separated regions, followed by postselection when one particle is found in each location. Consider a state of two independent identical qubits $|\psi_D\rangle = |\varphi_D \uparrow, \varphi'_D \downarrow\rangle$, where φ_D, φ'_D are spatial wave functions and $\uparrow, \downarrow$ are pseudospins. The result of applying sLOCC to $|\psi_D\rangle$ is [23]

$$|\psi_{LR}\rangle = \frac{lr' |L \uparrow, R \downarrow\rangle + e^{i\phi} rl' |L \downarrow, R \uparrow\rangle}{\sqrt{|lr'|^2 + |rl'|^2}}, \quad (1)$$

where l, l' (r, r') are the probability amplitudes for each particle to be found in the region L (R), while ϕ is the exchange (statistical) phase; $|\psi_{LR}\rangle$ is entangled only if the qubits spatially overlap, i.e., are spatially indistinguishable, in the regions L and R. Remarkably, the sLOCC process makes particle statistics emerge naturally in the final entangled state. The entanglement obtained is experimentally accessible [29,30], and has been exploited for teleportation [29] and phase discrimination [31]. Also, sLOCC-based indistinguishability is useful for protecting entanglement against noise [24,26–28].

Here we give further value to sLOCC by experimentally showing, in a quantum optical setup, that its theoretical framework enables a phase-estimation procedure to directly access the EPs of indistinguishable particles of any nature [Fig. 1(a)].

II. THEORETICAL FRAMEWORK

The conceptual procedure is depicted in Fig. 1(a). We take a pair of two-level identical particles, independently prepared and initially uncorrelated, whose spatial wave functions and pseudospins are $\varphi, \uparrow$ and $\varphi', \downarrow$, respectively. In the no-label formalism, we write this state as $|\psi_{\text{in}}\rangle = |\varphi \uparrow, \varphi' \downarrow\rangle$. Then, a deformation operation $|\varphi\rangle \rightarrow |\varphi_D\rangle$, $|\varphi'\rangle \rightarrow |\varphi'_D\rangle$ is performed [24,26,32] to distribute the spatial wave functions over two distinct regions L and R in a controllable way, thus transforming $|\psi_{\text{in}}\rangle$ into $|\psi_D\rangle = |\varphi_D \uparrow, \varphi'_D \downarrow\rangle$, where

$$|\varphi_D\rangle = l |L\rangle + r |R\rangle, \quad |\varphi'_D\rangle = l' |L\rangle + r' |R\rangle. \quad (2)$$

Here, the coefficients $l = \langle L|\varphi_D\rangle, l' = \langle L|\varphi'_D\rangle, r = \langle R|\varphi_D\rangle$, and $r' = \langle R|\varphi'_D\rangle$ are the tunable probability amplitudes of finding the particle whose spatial wave function is φ_D or φ'_D at the sites L and R, respectively.

To implement the sLOCC measurement, we perform postselected detection of the states, where exactly one
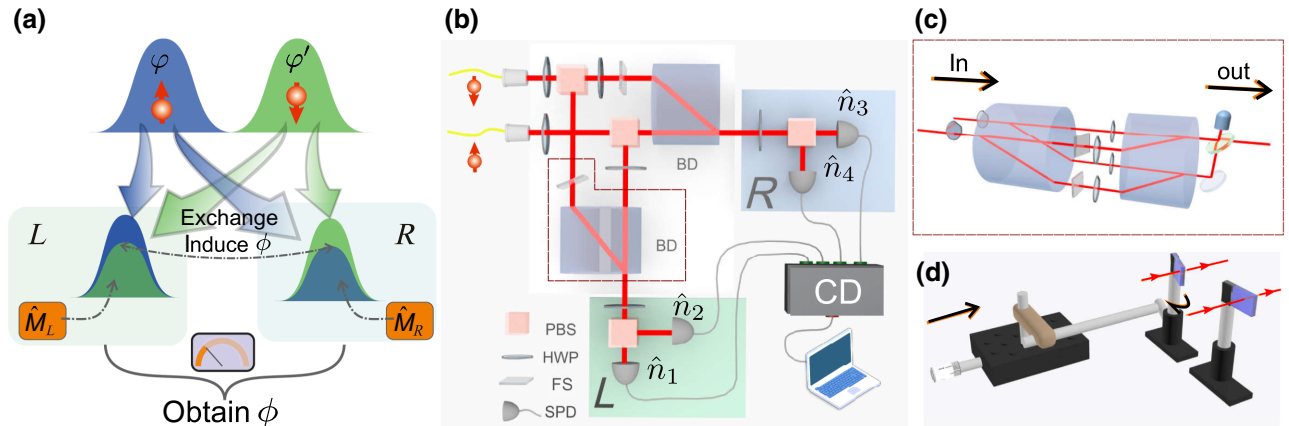

FIG. 1. Theoretical scheme and experimental setup. (a) Conceptual procedure. The wave functions of two identical particles are distributed over two distinct regions L and R and adjusted to spatially overlap, generating spatial indistinguishability. A sLOCC measurement is used to directly observe the EP using a single-particle rotation $\hat{M}$ in the two regions. (b) Experimental setup. Two independently prepared photons with opposite polarizations are distributed to two distinct spatial regions L and R. In each region, a beam displacer (BD) is used to merge two beams, generating spatial indistinguishability between the two photons. The relative phase between the two spatial modes of the photons is tuned using a phase-adjustment device consisting of fused silicon (FS), shown in (d). The four outputs are individually directed towards four single-photon detectors (SPDs), where a coincidence device (CD) is used to deal with the signals. PBS, polarization beam splitter; HWP, half-wave plate. (c) Replacement setup for the framed area in (b). An unbalanced interferometer is used to prepare mixed states.

qubit per region is recorded. In total, this last step amounts to projecting the state $|\psi_D\rangle$ onto the two-particle basis $\mathcal{B}_{LR} = \{|L \uparrow, R \uparrow\rangle, |L \uparrow, R \downarrow\rangle, |L \downarrow, R \uparrow\rangle, |L \downarrow, R \downarrow\rangle\}$ via the projection operator $\hat{\Pi}_{LR} = \sum_{\sigma,\tau=\uparrow,\downarrow} |L\sigma, R\tau\rangle \langle L\sigma, R\tau|$.

We recall that the two particles in the state $|\psi_D\rangle$ are indistinguishable in the eyes of the detectors. This means that it is not possible to know the region of space where each detected constituent comes from. This absence of which-way information is encoded in the result of the sLOCC operation, which is easily computed to be the (normalized) two-particle entangled state

$$
\begin{aligned}
|\psi_{LR}\rangle &= \frac{\hat{\Pi}_{LR} |\psi_D\rangle}{\sqrt{\langle \psi_D| \hat{\Pi}_{LR} |\psi_D\rangle}} \\
&= \frac{lr' |L \uparrow, R \downarrow\rangle + e^{i\phi} rl' |L \downarrow, R \uparrow\rangle}{\sqrt{|lr'|^2 + |rl'|^2}},
\end{aligned}
\tag{3}
$$

generated with probability $P_{LR} = |lr'|^2 + |rl'|^2$ [23]. The phase ϕ that emerges naturally in Eq. (3) is exactly the relative EP that we want to measure [Fig. 1(a)]. In fact, it is fundamentally contained in the probability amplitudes $\langle \chi_L, \chi_R| \psi_D\rangle = \langle \chi_L| \chi_D\rangle \langle \chi_R| \chi_D'\rangle + \eta \langle \chi_L| \chi_D'\rangle \langle \chi_R| \chi_D\rangle$ [21], where $\chi_L = L\sigma$, $\chi_R = R\tau$, $\chi_D = \varphi_D \uparrow$, and $\chi_D' = \varphi_D' \downarrow$, and $\eta = e^{i\phi}$ is the particle statistics parameter. It is worth highlighting that the state $|\psi_{LR}\rangle$ resulting from the sLOCC process describes two particles occupying two distinct regions of space, which are thus now distinguishable and individually addressable. The spatial indistinguishability $\mathcal{I}$ under sLOCC associated with the state $|\psi_D\rangle$, and thus with the state $|\psi_{LR}\rangle$, is given by [24]

$$
\begin{aligned}
\mathcal{I} = &-\frac{|lr'|^2}{|lr'|^2 + |l'r|^2} \log_2 \frac{|lr'|^2}{|lr'|^2 + |l'r|^2} \\
&-\frac{|l'r|^2}{|lr'|^2 + |l'r|^2} \log_2 \frac{|l'r|^2}{|lr'|^2 + |l'r|^2}.
\end{aligned}
\tag{4}
$$

In general, the state in Eq. (3) represents a quantum superposition of two-particle states whose relative phase contains the EP of the particles. Notice that one of the major difficulties in directly measuring the particle statistical phase consists in creating quantum interference between a given state and its counterpart where particles have been physically exchanged [14]. A so-called state-dependent transport protocol has been engineered with this aim [33] and successfully realized with photons [13]. On the other hand, in our scheme, the fundamental EP appears straightforwardly as a natural consequence of spatial overlap in separated regions plus the sLOCC procedure, making it amenable to being directly measured via individual operations on the particles. We proceed by rotating the pseudospin of both qubits by $\pi/4$. Given the single-particle

operator

$$
\hat{M}_X = \frac{1}{\sqrt{2}} \begin{pmatrix} 1 & -1 \\ 1 & 1 \end{pmatrix},
\tag{5}
$$

which performs this operation on the region $X = L, R$, the resulting state is given by $|\psi_f\rangle = \hat{M}_L \otimes \hat{M}_R |\psi_{LR}\rangle$. Finally, a direct measurement of the pseudospin along the z axis in both of the regions L and R provides information about the EP. We find that

$$
\langle \psi_f \left| \hat{\sigma}_L^z \otimes \hat{\sigma}_R^z \right| \psi_f \rangle = \frac{2lr'rl'}{|lr'|^2 + |rl'|^2} \cos\phi,
\tag{6}
$$

where we take the coefficients l, r, l', r' to be real, since we are able to directly control the distribution of the initial spatial wave functions over L and R during the preparation of the state $|\psi_D\rangle$. By knowing these amplitudes, it is thus possible to recover the value of the EP from repeated pseudospin measurements along the z axis.

Remarkably, the role of the spatial indistinguishability $\mathcal{I}$ emerges clearly from Eq. (6): as its value varies from $\mathcal{I} = 1$ (maximum indistinguishability, which is obtained, e.g., when $l = r = l' = r' = 1/\sqrt{2}$) to $\mathcal{I} = 0$ (distinguishable particles, e.g., when $l = r' = 1$, $l' = r = 0$) [24], the values assumed by Eq. (6) change continuously from $\cos\phi$ to zero, correspondingly. It follows that spatial indistinguishability not only is an essential element for measuring the EP with our procedure, but also acts as a sensitivity regulator that tunes our ability to access the value of ϕ.

III. EXPERIMENTAL DETAILS

Denoting by $|H\rangle$ and $|V\rangle$ the horizontal and vertical polarizations, respectively, of a photon, we make the correspondence $|H\rangle \leftrightarrow |\uparrow\rangle$ and $|V\rangle \leftrightarrow |\downarrow\rangle$. A pulsed ultraviolet beam with a wavelength of 400 nm is used to pump a type-II phase-matched β-barium borate crystal to generate two uncorrelated photons ($|H\rangle \otimes |V\rangle$) via spontaneous parametric down-conversion. Hong-Ou-Mandel interference is performed to characterize the indistinguishability of the two photons, providing a visibility of 97.7% [29]. Single-mode fibers collect the photons via fiber couplers and direct them towards the effective experimental setup illustrated in Fig. 1(b). Here, the weights of their horizontal and vertical polarizations are tuned using a pair of HWPs fixed at $22.5°$ and $-\beta/2$ (an adjustable angle). An additional pair of HWPs at $45°$ is placed in L to restore the original input polarizations. The result is the preparation of the state $|\psi_D\rangle$, with $|\varphi_D\rangle = (|L\rangle + |R\rangle)/\sqrt{2}$, $|\varphi_D'\rangle = \sin\beta |L\rangle + \cos\beta |R\rangle$.

Using a homemade phase-adjustment device composed of a thin plate of fused silicon fixed in R and another identical plate that is tilted and placed in L [Figs. 1(b) and 1(d)], an arbitrary relative phase ϕ_s is judiciously introduced between the components L and R of the photon

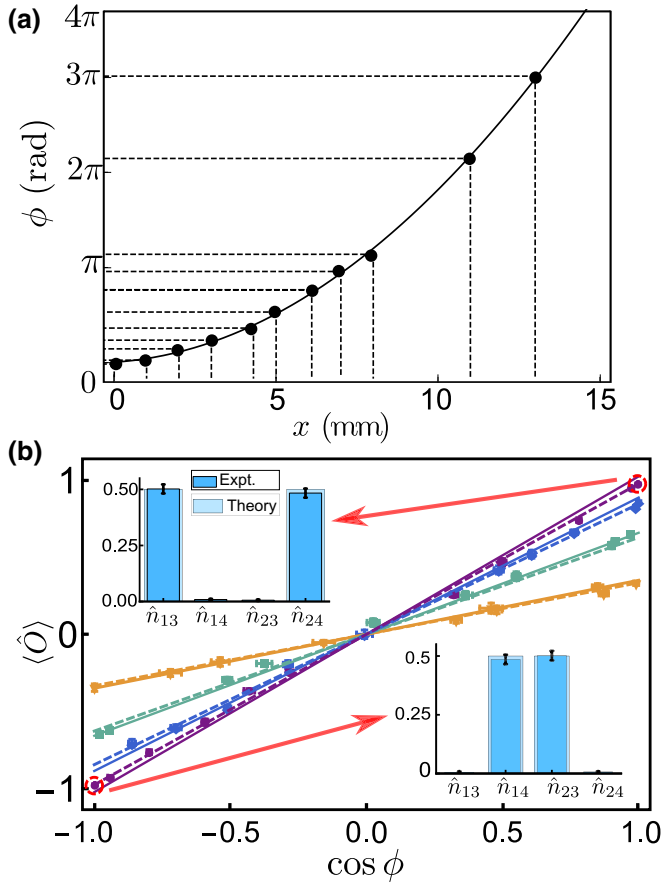FIG. 2. (a) Relation between the distance x of the movable plate from the place perpendicular to the beam and the generated relative phase ϕ. The black dots represent the experimental results, while the black curve is the theoretical prediction. The error bars are too small to be visible. (b) Relation between $\langle\hat{O}\rangle$ and $\cos\phi$. Results are reported for different values of β, where the purple, blue, green, and brown colors represent $\beta = 45°, 30°, 20°$, and $10°$, respectively. The solid lines represent the ideal expected results, while the dashed lines show the predictions when noise is taken into consideration. The experimental values are represented by markers. The two insets show the coincidence counts $\hat{n}_{13}, \hat{n}_{14}, \hat{n}_{23}$, and $\hat{n}_{24}$ for bosons and fermions.

state φ'_D, which becomes $|\varphi'_D\rangle = e^{i\phi_s}\sin\beta|L\rangle + \cos\beta|R\rangle$. As shown in Fig. 1(d), ϕ_s is tuned by directly adjusting distance x of the movable plate from the place perpendicular to the beam. The relation between ϕ_s and x is displayed in Fig. 2(a) by experimental results (dots) and a theoretical prediction (solid line) for a plate thickness $d = 199.94 \pm 1.43$ μm and a rotation radius $r = 102.36 \pm 0.91$ mm (see Appendix A).

A beam displacer is used to make the two beams overlap in both regions. We proceed by setting a HWP at $22.5°$ after the BD in both L and R to implement the desired rotation, producing the final state $|\psi_f\rangle$. The pseudospin measurement $\hat{\sigma}_z^{(L)} \otimes \hat{\sigma}_z^{(R)}$ is then performed as a coincidence-counting measurement by placing each PBS

in both of the regions L and R. Each output of the PBSs is individually directed towards a single-photon detector. The corresponding measured observable is

$$\langle\hat{O}\rangle = \hat{n}_{13} + \hat{n}_{24} - \hat{n}_{14} - \hat{n}_{23}, \tag{7}$$

where $\hat{n}_{ij}$ is the coincidence count between the outputs $\hat{n}_i$ and $\hat{n}_j$, which are shown in Fig. 1(b). This spatially localized operation, implemented through local counting in L and R, and classical communication tools, realized via the coincidence device, create the state in Eq. (1) with $l = r = 1/\sqrt{2}$, $l' = \sin\beta$, and $r' = \cos\beta$, i.e.,

$$|\psi_{LR}\rangle = \cos\beta|LH, RV\rangle + e^{i\phi_s}\sin\beta|LV, RH\rangle, \tag{8}$$

before the final rotation transforms it into $|\psi_f\rangle$. Notice that the relative phase ϕ_s in Eq. (8) plays the exact same role as the real EP ϕ in Eq. (3) (which is set to zero here, since our experiment is run with bosons). Changing ϕ_s amounts to simulating the behavior of identical particles with different natures. In other words, the ability of our setup to directly measure ϕ_s provides strong evidence that it can directly detect the EP of any type of particle. Renaming the simulated exchange phase as ϕ, we obtain

$$\langle\hat{O}\rangle \equiv \langle\psi_f|\hat{O}|\psi_f\rangle = \sin(2\beta)\cos\phi, \tag{9}$$

from which ϕ can be easily obtained.

We set $\beta = 45°$ and $\phi = 0$ to prepare two maximally indistinguishable photons (bosons), generating a maximum entanglement $|\psi_{LR}\rangle = (|LH, RV\rangle + |LV, RH\rangle)/\sqrt{2}$ with a fidelity of 0.99 ± 0.01. Unavoidable experimental errors prevent achievement of the ideal maximum indistinguishability, which leads to nonoptimal performance of the real setup. Following the method used in Ref. [13], we treat such errors as a constant factor affecting the final experimental results. We assume that the experimentally prepared state is the desired (ideal) one with probability F, while errors give rise to a spoiled state with probability $1 - F$. Within this model, the spoiled state does not contribute to the expectation value of $\hat{O}$, leading to the experimentally measured expectation value $\langle\hat{O}\rangle_e = F\langle\hat{O}\rangle_i$, where $\langle\hat{O}\rangle_i$ is the ideal prediction. By preparing several states of the type represented by Eq. (8) for different values of ϕ, we use quantum state tomography [34] to estimate the probability to be $F = 0.977$ (see Appendix B).

The two insets in Fig. 2(b) show the coincidence counts $\hat{n}_{13}, \hat{n}_{14}, \hat{n}_{23}$, and $\hat{n}_{24}$ for the cases of (real) bosons and (simulated) fermions, with $\beta = 45°$. Treating experimental errors in the manner introduced above, we obtain $\phi_b = 0.04 \pm 0.06$ for bosons and $\phi_f = 3.12 \pm 0.05$ for fermions, which match well with their expected EPs. Here, the error bars show the standard deviation, which is estimated based on the experimental data via a Monte Carlo method.

As shown in Fig. 2(b), by varying the angle β, we implement various spatial overlaps to provide deeper insights into the role played by spatial indistinguishability in our scheme, and adjust the EPs (including anyonic ones) with the homemade device. The detected values of $\langle \hat{O} \rangle$ are given as a function of $\cos \phi$, where ϕ is obtained via tomographic measurements, for different degrees of spatial overlap and, hence, of the spatial indistinguishability $\mathcal{I} = -\sin^2 \beta \log_2(\sin^2 \beta) - \cos^2 \beta \log_2(\cos^2 \beta)$ [24]. The experimental results match quite well with the theoretical predictions. In particular, the case of $\beta = 45°$ corresponds to the maximum spatial overlap ($\mathcal{I} = 1$), while $\beta = 30°$, $\beta = 20°$, and $\beta = 10°$ are associated with partial spatial overlaps ($\mathcal{I} < 1$). Notice that when $\mathcal{I}$ decreases, the ranges of values of $\langle \hat{O} \rangle$ decrease accordingly, leading to a lower sensitivity. Spatial indistinguishability acts as a sensitive regulator governing the range of measured values.

As an extension of our framework, we analyze the scenario where the input is a flux of particle pairs whose exchange phase is known to be either ϕ_1 with probability p or ϕ_2 with probability $1-p$. Each two-particle state is thus given by the classical mixture

$$\rho = p |\psi_1\rangle \langle\psi_1| + (1-p) |\psi_2\rangle \langle\psi_2|, \qquad (10)$$

where $|\psi_1\rangle = \cos \beta |LH, RV\rangle + e^{i\phi_1} \sin \beta |LV, RH\rangle$ and $|\psi_2\rangle = \cos \beta |LH, RV\rangle + e^{i\phi_2} \sin \beta |LV, RH\rangle$. We now want to exploit our procedure to estimate the probability distribution p of the two types of particles by directly measuring their EPs.

To prepare ρ, we replace the framed area in Fig. 1(b) with the unbalanced interferometer shown in Fig. 1(c). Here, a BD equipped with two HWPs separately placed in each beam is used to split each beam into two vertical beams. The two upper arms are used to prepare a particle with EP ϕ_1, while the two lower arms are used to prepare a particle with EP ϕ_2. By changing the angles of the two HWPs before the BD, the probability distributions p can be adjusted. As mentioned above, the EPs ϕ_1 and ϕ_2 are regulated with the corresponding homemade phase-adjustment devices. Then, another BD, together with several HWPs, combines the two upper (lower) arms into one beam horizontally. Finally, the two beams are combined with a beam splitter, in which the desired classical mixed state of Eq. (10) is generated in one output and the other output is blocked.

The expectation value $\langle \hat{O} \rangle = \text{Tr}[\rho \hat{O}] = p \langle\psi_1| \hat{O} |\psi_1\rangle + (1-p) \langle\psi_2| \hat{O} |\psi_2\rangle$ is measured following the same method as that introduced above. For simplicity, we assume that the values of ϕ_1 and ϕ_2 are provided as prior information, leading to a reduction in $\langle \hat{O} \rangle$ as a linear function of p. Notice that if this is not the case, the values of ϕ_1 and ϕ_2 can nonetheless be obtained by our procedure by directly measuring them on a sufficiently large sample of particles. We start with $\phi_1 = 0$ and $\phi_2 = \pi/2$ to investigate
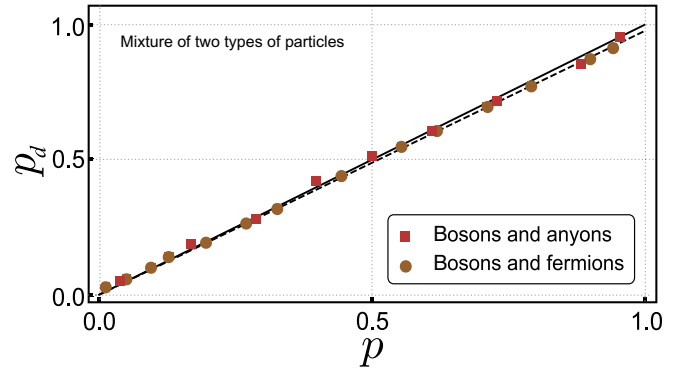

FIG. 3. Probability distribution p_d for a mixture of two types of particles measured by our procedure versus the value p directly generated by rotating the HWPs. Experimental results for a mixture of bosons and anyons with EP $\phi = \pi/2$ (red markers), and for a mixture of bosons and fermions (brown markers). The solid lines represent the ideal expected values, while the dashed lines are the theoretical predictions when noise is considered. The error bars are too small to be visible.

a classical mixture of bosons and anyons with $\beta = 45°$. We generate different probability distributions p by rotating the two HWPs before the first BD, as shown in Fig. 1(c). Also, we set $\phi_2 = \pi$ to investigate a mixture of bosons and fermions. The results are reported in Fig. 3, where the detected probability distributions p_d, obtained based on the measured values of $\langle \hat{O} \rangle$, are shown versus the values of p directly generated by rotating the HWPs. Excellent agreement with the theoretical predictions is observed (see Appendix C). This last experiment demonstrates how our procedure can be used to obtain information about the probability distribution p for a mixture of two known different types of particles. If the number of types of particles is increased or unknown, a complete characterization of the incoming flux can still be done by directly measuring the various EPs of particle pairs making up a sufficiently large sample.

IV. DISCUSSION

In summary, we show experimentally that the sLOCC framework is inherently amenable to direct measurement of the EP of indistinguishable particles. The particle statistics in the measured state are entirely due to the spatial indistinguishability achieved via the deformation of particle wave packets. The sLOCC process functions as a trigger that makes the EP directly accessible within the entanglement generated. For this reason, physical exchange of particles and the related geometric phase do not occur here, in contrast with the technique previously adopted [13] to measure the bosonic EP of photons. Our procedure works for bosons, fermions, and anyons. We judiciously design the optical setup to simulate various particle statistics: differently from other methods used for

this purpose in the context of photonic quantum walks [35,36], we manually inject different EPs by accurately tuning a phase-adjustment device, always observing agreement between the measured values and predictions. Our apparatus confirms the real bosonic (symmetric) nature of photons, including the result of Ref. [13]. We also prove that repeated measurements of the EP permit us to reconstruct the probability distribution for statistical mixtures of states of particles of different nature. Our work provides a general scheme to directly explore the symmetrization principle and the role of particle statistics in various contexts, which should have extendable applications in other phase-measurement schemes [37–39].

In the future, it would be interesting to apply our setup on nonoptical platforms to achieve the direct measurement of real (not simulated) fermionic and anyonic EPs. In fact, our scheme can be translated to any platform that implements linear optics, such as platforms for electronic optics [40], where the degree of indistinguishability can be adjusted by use of quantum point contacts acting as electronic beam splitters [41]. Additionally, quantum dots appear promising for on-demand generation of single electrons [42], including their initialization and coherent control [43,44], where the tunnel effect in double quantum dots could play the role of the deformation operation generating the indistinguishability [32,45].

We also envisage possible practical applications of our protocol to measure the EP of anyons in topological quantum computers [4,46,47]. Furthermore, the proposed theoretical and experimental setup can be easily adapted to find application in a phase-estimation protocol aided by indistinguishability. Suppose that instead of postselecting the states where exactly one qubit per region is found in the sLOCC measurement, we discard these states by postselecting the complementary ones. This amounts to projecting the state $|\psi_D\rangle$ onto the two-particle basis $\mathcal{B}_{XX} = \{|X\uparrow, X\uparrow\rangle, |X\uparrow, X\downarrow\rangle, |X\downarrow, X\downarrow\rangle\}$, with $X = L, R$. The resulting state is thus

$$|\psi_{XX}\rangle = \frac{ll'\,|L\uparrow, L\downarrow\rangle + rr'\,|R\uparrow, R\downarrow\rangle}{\sqrt{|ll'|^2 + |rr'|^2}}, \qquad (11)$$

which, as can be noticed by rewriting it in the Fock representation and disregarding the pseudospin, is equivalent to

$$|\psi_{XX}\rangle = \frac{ll'\,|2,0\rangle + rr'\,|0,2\rangle}{\sqrt{|ll'|^2 + |rr'|^2}}. \qquad (12)$$

This is NOON-like states exploitable for quantum-enhanced phase estimation [48–50]. By adjusting the values of the coefficients, one may obtain NOON states with various weights for the terms $|2,0\rangle$ and $|0,2\rangle$. Remarkably, since the only difference from the EP measurement scheme

is in the postselection, this state can be experimentally generated with the same setup as that depicted in Fig. 1(b) (excluding the final measurement step).

Finally, we highlight that while the sLOCC operational framework is exploited here to achieve a result of fundamental interest, different practical applications have been designed and experimentally implemented in fields ranging from quantum communication to quantum metrology and sensing, including the generation of entanglement between identical constituents [23,29], the protection of quantum correlations from detrimental external noise [24,26–28], and the generation of quantum coherence for metrological applications [25,31].

APPENDIX A: INTRODUCTION OF PHASE ADJUSTMENT

For a better and more intuitive understanding of the subtle features of the adjustment of the EP ϕ, we aim here to derive an intuitive geometrical relationship between the distance x moved by the moving plate and the corresponding EP ϕ. This should help us to further connect the distance of movement x with the direct observable $\hat{O}$, by exploiting our experimental setup's capability to obtain the exact phase of the EP directly.

Here, the corresponding EP of the simulated identical particles ranges from 0 to π. The necessary experimental initialization starts from the adjustment to obtain $\phi = 0$ with two photons separately passing perpendicularly through two thin plates of fused silicon (both having the same thickness d), of which one is motionless and the other can be rotated by a small angle. This rotation is driven by a movable plate (MP). The thickness d is about 200 μm, so that the moving part has no influence on the parts of the setup that follow. At each displacement, a tomography procedure is performed so as to construct the corresponding density matrix and, furthermore, to confirm the relative phase ϕ [34]. The experimental results are represented in
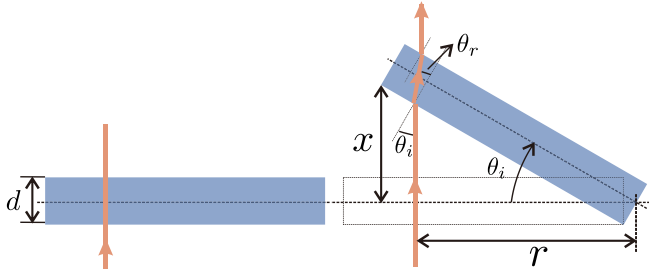
FIG. 4. Sketch of the tilted experimental setup.

Fig. 2(a), in which the associated error bars are too small to see.

Here, we determine the theoretical predictions based on our experimental setup. As shown in Fig. 4, the incidence angle θ_i and the refraction angle θ_r satisfy the refraction law, where the refractive index of the glass sheet is $n = 1.5$ and the refractive index of air is $n_0 = 1$. We can assume $x = r \sin \theta_i$ for a small angle θ_i. The relationship between the distance of movement x and the phase ϕ is

$$
\phi = \frac{2\pi}{\lambda} nd \left(\frac{1}{\sqrt{1 - (\sin \theta_i n_0/n)^2}} - 1 \right)
$$
$$
= \frac{2\pi}{\lambda} nd \left(\frac{1}{\sqrt{1 - (x/rn)^2}} - 1 \right), \tag{A1}
$$

where λ corresponds to the wavelength of the photon. Moreover, we find that the parameters d and r are $d = 199.94 \pm 1.43$ μm and $r = 102.36 \pm 0.91$ mm. These numbers are in agreement with the measured values, and fit well with our experimental results presented in Fig. 2(a). This means that we can straightforwardly obtain the EP ϕ through the displacement of the MP x, which is a more intuitive quantity than ϕ. Also, we can exploit the direct measurement results between the observable $\hat{O}$ and x instead of between $\hat{O}$ and ϕ; see Fig. 5. Based on Eq. (A1), ϕ can be adjusted to be larger than π; however, considering its periodicity, it can be transformed to a value that is within the range $[0,\pi]$.

APPENDIX B: TREATMENT OF EXPERIMENTAL ERRORS AND PREDICTION OF PERFORMANCE OF THE SETUP

The temporal indistinguishability characterizing the two photons in our setup is evaluated by measuring the Hong-Ou-Mandel interference dip, showing a visibility of 97.7%. This incomplete indistinguishability is the result of unavoidable environmental decoherence and of the somewhat limited performance of our experimental setup, e.g., the effects of white noise and dark counts, leading to the generation of states that deviate slightly from the ideal ones. Similarly to Ref. [13], we model these experimental
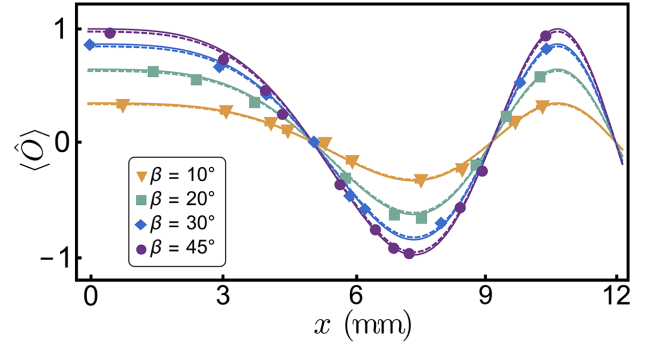

FIG. 5. Experimental results for different simulated types of particles. Measured values of $\langle \hat{O} \rangle$ versus the displacement x of the moving plate, generating a relative phase ϕ in the range from 0 to π. Results are reported for different values of β (different colors), corresponding to different degrees of spatial indistinguishability. The solid lines represent the theoretically expected results in the ideal (no-noise) scenario, while the dashed lines show the theoretical values when noise is taken into consideration. The experimentally measured values are represented by markers.

errors as a constant factor and compute the estimated performance of our setup.

The ideal state that we would like to prepare is

$$
|\psi_{LR}\rangle = \cos \beta \, |LH, RV\rangle + e^{i\phi} \sin \beta \, |LV, RH\rangle, \tag{B1}
$$

where ϕ represents the simulated EP, while β characterizes the degree of spatial indistinguishability. Denoting by ρ_i the corresponding pure-state density matrix, i.e., $\rho_i = |\psi_{LR}\rangle \langle \psi_{LR}|$, we model the experimental errors as if they would lead to the generation of the ideal state ρ_i with probability F. If we use ρ_n to denote the noisy state otherwise achieved, obtained with probability $1 - F$, the setup thus generates the mixed state

$$
\rho_e = F \rho_i + (1 - F) \rho_n. \tag{B2}
$$

We consider the noisy part as composed of two contributions: a state ρ_{n1} accounting for white noise due to accidental errors,

$$
\rho_{n1} = \frac{1}{4} (|LH, RH\rangle \langle LH, RH| + |LH, RV\rangle \langle LH, RV| \\
+ |LV, RH\rangle \langle LV, RH| + |LV, RV\rangle \langle LV, RV|), \tag{B3}
$$

and a state ρ_{n2} accounting for decoherence effects,

$$
\rho_{n2} = \frac{1}{2} (|LH, RV\rangle \langle LH, RV| + |LV, RH\rangle \langle LV, RH|). \tag{B4}
$$

The complete noisy state generated is thus given by

$$
\rho_n = a \rho_{n1} + b \rho_{n2},
$$

where the coefficients a and b are such that $a + b = 1$.

It is now easy to show that, once it has been rotated as described in the main text, the noisy component does not contribute to the expectation value of the observable $\hat{O} = \hat{\sigma}_L^z \otimes \hat{\sigma}_R^z$ that we want to measure. As a consequence, the only relevant effect of the experimental errors within this model is to reduce the visibility of the two indistinguishable photons, meaning that the experimental results $\langle \hat{O} \rangle_e$ are related to the ideal ones $\langle \hat{O} \rangle_i$ by $\langle \hat{O} \rangle_e = F \langle \hat{O} \rangle_i$.

We now want to estimate the parameter F. To do so, we use quantum tomography to experimentally reconstruct ρ_e for different states generated while varying ϕ from 0 to π [34]. This allows us to compute ϕ and β, from which the ideal state Eq. (B1) can be reconstructed. After preparing several experimental states and obtaining the corresponding groups of ϕ and β, we use Eq. (B2) to get $F = 0.977$. As for the noisy part ρ_n, composed of ρ_{n1} and ρ_{n2}, the values of a and b make little difference. Remarkably, we find that the parameter F is affected by fluctuations whose magnitude is of the order of 10^{-3}.

The treatment of the experimental errors presented above is exploited in the main text to perform direct measurement of the EP with higher accuracy.

APPENDIX C: FURTHER EXPERIMENTAL PLOTS

By changing the angle β of the HWP, we measure various simulated phases (including anyonic ones) for different values of the spatial overlap in order to obtain further insights into the role played by spatial indistinguishability in our framework. The results are shown in Fig. 5. Here, the measured values of $\langle \hat{O} \rangle$ are given directly as a function of the movable plate's displacement for different degrees of spatial overlap and, thus, of the spatial indistinguishability $\mathcal{I}$. The latter is defined by an entropic expression in terms of the probabilities of finding each particle in a given region [24] and, in our experiment, reads $\mathcal{I} = -\sin^2 \beta \log_2(\sin^2 \beta) - \cos^2 \beta \log_2(\cos^2 \beta)$. We recall that $\beta = 45°$ corresponds to the maximum spatial overlap (i.e., the maximum spatial indistinguishability $\mathcal{I} = 1$), while $\beta = 30°$, $\beta = 20°$, and $\beta = 10°$ denote partial spatial overlap ($\mathcal{I} < 1$). The experimental results are reported by markers of different types, while the solid lines represent the ideal theoretically expected values $\langle \hat{O} \rangle_i$. Finally, the dashed lines correspond to the values $\langle \hat{O} \rangle_e$ expected when the experimental errors are taken into consideration. Notice that, as previously discussed, when the degree of spatial indistinguishability decreases, the ranges of values assumed by $\langle \hat{O} \rangle$ decrease accordingly, thus leading to a lower sensitivity.

In performing the second experiment, for the classical mixture of two types of particles, we set $\beta = 45°$ for simplicity, as reported in the main text. To begin with, we set $\phi_1 = 0$ and $\phi_2 = \pi/2$ to simulate a classical mixture of
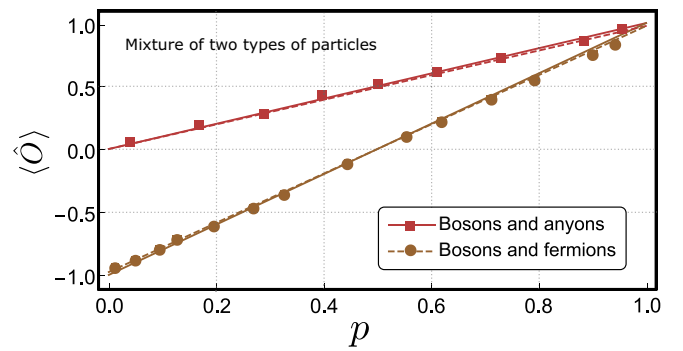

FIG. 6. Relation between $\langle \hat{O} \rangle$ and the simulated probability distribution p of a mixture of bosons and anyons with EP $\phi = \pi/2$ (red) and one of bosons and fermions (brown). The solid lines represent the ideal expected values, the dashed lines represent the theoretically expected values when noise is considered, and the markers represent the experimentally obtained results. The error bars are too small to be visible.

bosons and anyons. We simulate different probability distributions by rotating the two input HWPs shown in Fig. 1. The expectation value of $\hat{O}$, given by

$$\langle \hat{O} \rangle = \text{Tr}[\rho \, \hat{O}] = p \, \langle \psi_1 | \, \hat{O} \, | \psi_1 \rangle + (1-p) \, \langle \psi_2 | \, \hat{O} \, | \psi_2 \rangle, \tag{C1}$$

is measured as in the pure-state scenario. For simplicity, we assume that the values of ϕ_1 and ϕ_2 are given as prior information, allowing us to compute the expectation values $\langle \psi_j | \, \hat{O} \, | \psi_j \rangle$, $j = 1, 2$, and reducing Eq. (C1) to one linear equation in p. Notice that if this is not the case, the values of ϕ_1 and ϕ_2 can nonetheless be obtained by exploiting our procedure to directly measure them on a sufficiently large sample of particle pairs.

The results obtained are represented by red markers in Fig. 6, where $\langle \hat{O} \rangle$ is plotted against the simulated probability p. Here, the efficacy of our setup is apparent when compared with the red solid line, representing the theoretically expected values of $\langle \hat{O} \rangle$ computed using Eq. (C1). As before, the dashed line represents the theoretical values expected when the action of noise is considered, i.e., $\langle \hat{O} \rangle_e = F \langle \hat{O} \rangle$. Then, we set $\phi_2 = \pi$ to simulate a mixture of bosons and fermions and repeat the experiment. The results, displayed in Fig. 6 by brown markers and lines, are once again in good agreement with our theoretical predictions.

[1] A. Peres, *Quantum Theory: Concepts and Methods* (Kluwer Academic Publishers, New York, 2002).

[2] J. M. Leinaas and J. Myrheim, On the theory of identical particles, Il Nuovo Cimento B (1971-1996) **37**, 1 (1977).

[3] F. Wilczek, Magnetic Flux, Angular Momentum, and Statistics, Phys. Rev. Lett. **48,** 1144 (1982).

[4] C. Nayak, S. H. Simon, A. Stern, M. Freedman, and S. Das Sarma, Non-Abelian anyons and topological quantum computation, Rev. Mod. Phys. **80,** 1083 (2008).

[5] J. Nakamura, S. Liang, G. C. Gardner, and M. J. Manfra, Direct observation of anyonic braiding statistics, Nat. Phys. **16,** 931 (2020).

[6] H. Bartolomei, M. Kumar, R. Bisognin, A. Marguerite, J. M. Berroir, E. Bocquillon, B. Placais, A. Cavanna, Q. Dong, U. Gennser, Y. Jin, and G. Fève, Fractional statistics in anyon collisions, Science **368,** 173 (2020).

[7] R. C. Hilborn and C. L. Yuca, Spectroscopic Test of the Symmetrization Postulate for Spin-0 Nuclei, Phys. Rev. Lett. **76,** 2844 (1996).

[8] G. Modugno, M. Inguscio, and G. M. Tino, Search for Small Violations of the Symmetrization Postulate for Spin-0 Particles, Phys. Rev. Lett. **81,** 4790 (1998).

[9] D. English, V. V. Yashchuk, and D. Budker, Spectroscopic Test of Bose-Einstein Statistics for Photons, Phys. Rev. Lett. **104,** 253604 (2010).

[10] K. Deilamian, J. D. Gillaspy, and D. E. Kelleher, Search for Small Violations of the Symmetrization Postulate in an Excited State of Helium, Phys. Rev. Lett. **74,** 4787 (1995).

[11] M. de Angelis, G. Gagliardi, L. Gianfrani, and G. M. Tino, Test of the Symmetrization Postulate for Spin-0 Particles, Phys. Rev. Lett. **76,** 2840 (1996).

[12] S. Ospelkaus, K. K. Ni, D. Wang, M. H. G. de Miranda, B. Neyenhuis, G. Quéméner, P. S. Julienne, J. L. Bohn, D. S. Jin, and J. Ye, Quantum-state controlled chemical reactions of ultracold potassium-rubidium molecules, Science **327,** 853 (2010).

[13] K. Tschernig, C. Müller, M. Smoor, T. Kroh, J. Wolters, O. Benson, K. Busch, and A. Pérez Leija, Direct observation of the particle exchange phase of photons, Nat. Photon. **15,** 671 (2021).

[14] R. Lo Franco, Directly proving the bosonic nature of photons, Nat. Photon. **15,** 638 (2021).

[15] M. C. Tichy, F. Mintert, and A. Buchleitner, Essential entanglement for atomic and molecular physics, J. Phys. B: At. Mol. Opt. Phys. **44,** 192001 (2011).

[16] G. C. Ghirardi and L. Marinatto, General criterion for the entanglement of two indistinguishable particles, Phys. Rev. A **70,** 012109 (2004).

[17] A. P. Balachandran, T. R. Govindarajan, A. R. de Queiroz, and A. F. Reyes-Lega, Entanglement and Particle Identity: A Unifying Approach, Phys. Rev. Lett. **110,** 080503 (2013).

[18] T. Sasaki, T. Ichikawa, and I. Tsutsui, Entanglement of indistinguishable particles, Phys. Rev. A **83,** 012113 (2011).

[19] F. Benatti, R. Floreanini, and U. Marzolino, Bipartite entanglement in systems of identical particles: The partial transposition criterion, Ann. Phys. **327,** 1304 (2012).

[20] S. Chin and J. Huh, Entanglement of identical particles and coherence in the first quantization language, Phys. Rev. A **99,** 052345 (2019).

[21] R. Lo Franco and G. Compagno, Quantum entanglement of identical particles by standard information-theoretic notions, Sci. Rep. **6,** 20603 (2016).

[22] G. Compagno, A. Castellini, and R. Lo Franco, Dealing with indistinguishable particles and their entanglement, Phil. Trans. R. Soc. A **376,** 20170317 (2018).

[23] R. Lo Franco and G. Compagno, Indistinguishability of Elementary Systems as a Resource for Quantum Information Processing, Phys. Rev. Lett. **120,** 240403 (2018).

[24] F. Nosrati, A. Castellini, G. Compagno, and R. Lo Franco, Robust entanglement preparation against noise by controlling spatial indistinguishability, Npj Quant. Inf. **6,** 39 (2020).

[25] A. Castellini, R. Lo Franco, L. Lami, A. Winter, G. Adesso, and G. Compagno, Indistinguishability-enabled coherence for quantum metrology, Phys. Rev. A **100,** 012308 (2019).

[26] M. Piccolini, F. Nosrati, G. Compagno, P. Livreri, R. Morandotti, and R. Lo Franco, Entanglement robustness via spatial deformation of identical particle wave functions, Entropy **23,** 708 (2021).

[27] F. Nosrati, A. Castellini, G. Compagno, and R. Lo Franco, Dynamics of spatially indistinguishable particles and quantum entanglement protection, Phys. Rev. A **102,** 062429 (2020).

[28] M. Piccolini, F. Nosrati, R. Morandotti, and R. Lo Franco, Indistinguishability-enhanced entanglement recovery by spatially localized operations and classical communication, Open Syst. Inf. Dyn. **28,** 2150020 (2021).

[29] K. Sun, Y. Wang, Z. H. Liu, X. Y. Xu, J. S. Xu, C. F. Li, G. C. Guo, A. Castellini, F. Nosrati, G. Compagno, and R. Lo Franco, Experimental quantum entanglement and teleportation by tuning remote spatial indistinguishability of independent photons, Opt. Lett. **45,** 6410 (2020).

[30] M. R. Barros, S. Chin, T. Pramanik, H. T. Lim, Y. W. Cho, J. Huh, and Y. S. Kim, Entangling bosons through particle indistinguishability and spatial overlap, Opt. Express **28,** 38083 (2020).

[31] K. Sun, Z. H. Liu, Y. Wang, Z. Y. Hao, X. Y. Xu, J. S. Xu, C. F. Li, G. C. Guo, A. Castellini, L. Lami, A. Winter, G. Adesso, G. Compagno, and R. Lo Franco, Activation of indistinguishability-based quantum coherence for enhanced metrological applications with particle statistics imprint, PNAS **119,** e2119765119 (2022).

[32] M. Piccolini, F. Nosrati, G. Adesso, R. Morandotti, and R. Lo Franco, Generating indistinguishability within identical particle systems: Spatial deformations as quantum resource activators, Phil. Trans. R. Soc. A, in press. Preprint at arXiv:2205.12136 [quant-ph] (2022).

[33] C. F. Roos, A. Alberti, D. Meschede, P. Hauke, and H. Häffner, Revealing Quantum Statistics with a Pair of Distant Atoms, Phys. Rev. Lett. **119,** 160401 (2017).

[34] D. F. V. James, P. G. Kwiat, W. J. Munro, and A. G. White, Measurement of qubits, Phys. Rev. A **64,** 052312 (2001).

[35] L. Sansoni, F. Sciarrino, G. Vallone, P. Mataloni, A. Crespi, R. Ramponi, and R. Osellame, Two-Particle Bosonic-Fermionic Quantum Walk via Integrated Photonics, Phys. Rev. Lett. **108,** 010502 (2012).

[36] J. C. Matthews, K. Poulios, J. D. Meinecke, A. Politi, A. Peruzzo, N. Ismail, K. Wörhoff, M. G. Thompson, and J. L. O'Brien, Observing fermionic statistics with photons in arbitrary processes, Sci. Rep. **3,** 1539 (2013).

[37] T. Krisnanda, S. Ghosh, T. Paterek, W. Laskowski, and T. C. H. Liew, Phase Measurement Beyond the Standard Quantum Limit Using a Quantum Neuromorphic Platform, Phys. Rev. Appl. **18,** 034011 (2022).

[38] S. Taravati and G. V. Eleftheriades, Low-Noise and Linear Nonmagnetic Circulator by a Temporal Nonreciprocal Phase Shifter, Phys. Rev. Appl. **18,** 034082 (2022).

[39] R. Wang, S. He, and H. Luo, Photonic Spin-Hall Differential Microscopy, Phys. Rev. Appl. **18,** 044016 (2022).

[40] C. Bäuerle, D. C. Glattli, T. Meunier, F. Portier, P. Roche, P. Roulleau, S. Takada, and X. Waintal, Fault-tolerant quantum computation by anyons, Rep. Prog. Phys. **81,** 056503 (2018).

[41] E. Bocquillon, V. Freulon, J. M. Berroir, P. Degiovanni, B. Plaçais, A. Cavanna, Y. Jin, and G. Fève, Coherence and indistinguishability of single electrons emitted by independent sources, Science **339,** 1054 (2013).

[42] G. Fève, A. Mahé, J. M. Berroir, T. Kontos, B. Placais, D. Glattli, A. Cavanna, B. Etienne, and Y. Jin, An on-demand coherent single-electron source, Science **316,** 1169 (2007).

[43] D. Press, T. D. Ladd, B. Zhang, and Y. Yamamoto, Complete quantum control of a single quantum dot spin using ultrafast optical pulses, Nature **456,** 218 (2008).

[44] J. R. Petta, A. C. Johnson, J. M. Taylor, E. A. Laird, A. Yacoby, M. D. Lukin, C. M. Marcus, M. P. Hanson, and A. C. Gossard, Coherent manipulation of coupled electron spins in semiconductor quantum dots, Science **309,** 2180 (2005).

[45] R. Hanson, L. P. Kouwenhoven, J. R. Petta, S. Tarucha, and L. M. K. Vandersypen, Spins in few-electron quantum dots, Rev. Mod. Phys. **79,** 1217 (2007).

[46] A. Y. Kitaev, Fault-tolerant quantum computation by anyons, Ann. Phys. **303,** 2 (2003).

[47] B. Field and T. Simula, Introduction to topological quantum computation with non-Abelian anyons, Quantum Sci. Technol. **3,** 045004 (2018).

[48] V. Giovannetti, S. Lloyd, and L. Maccone, Advances in quantum metrology, Nat. Photon. **5,** 222 (2011).

[49] M. Hiekkamäki, R. F. Barros, M. Ornigotti, and R. Fickler, Observation of the quantum Gouy phase, Nat. Photon. **16,** 828 (2022).

[50] S. Hong, J. Rehman, Y. S. Kim, Y. W. Cho, S. W. Lee, H. Jung, S. Moon, S. W. Han, and H. T. Lim, Quantum enhanced multiple-phase estimation with multi-mode *NOON* states, Nat. Commun. **12,** 5211 (2021).